

Spin-wave dispersion in $\text{CoCl}_2 \cdot 2\text{D}_2\text{O}$: A system of weakly coupled Ising chains

J. K. Kjems and J. Als-Nielsen

Danish Atomic Energy Commission Research Establishment, Risø, DK-4000 Roskilde, Denmark

Hans Fogedby*

Institut Laue-Langevin, BP 156 Centre de tri, 38042 Grenoble, Cedex, France

(Received 2 June 1975)

Inelastic neutron scattering has been used to study the magnetic excitation spectrum of $\text{CoCl}_2 \cdot 2\text{D}_2\text{O}$ in the antiferromagnetically ordered state. The results are analyzed in terms of a model of weakly interacting chains. The dominating interaction is the ferromagnetic Ising coupling along the chains although a comparison to optical studies shows that the Heisenberg nature of the interaction is larger than expected. The transverse anisotropy is found to be confined to relatively small wave vectors indicating that the responsible mechanism has long range in real space. The bound-state magnon branches were not observed.

I. INTRODUCTION

The anisotropic crystal structure of the magnetic salt $\text{CoCl}_2 \cdot 2\text{D}_2\text{O}$ ($\text{CoCl}_2 \cdot 2\text{H}_2\text{O}$) gives rise to several unique features in the magnetic excitation spectrum of this material. The Co^{2+} ions form chains along the crystallographic c axis, and the low point symmetry ($2/m$) of the crystalline electric field results in a Kramers doublet ground state.¹ The magnetic-susceptibility tensor of the ground state has a pronounced uniaxial anisotropy with easy magnetization along the crystallographic b^* -axis. The dominating magnetic interaction is the superexchange via Cl^- along the chains^{1,2} and hence $\text{CoCl}_2 \cdot 2\text{D}_2\text{O}$ (CC2) belongs to the class of pseudo-one-dimensional magnetic materials such as $(\text{CD}_3)_4\text{NMnCl}_3$ (TMMC),³ $\text{CsMnCl}_3 \cdot 2\text{H}_2\text{O}$,⁴ and CsNiF_3 .⁵ These systems are the real counterparts to various theoretical models. TMMC (Ref. 3) and $\text{CsMnCl}_3 \cdot 2\text{H}_2\text{O}$ (Ref. 4) can be described as classical linear-chain Heisenberg antiferromagnets, and CsNiF_3 is a linear-chain Heisenberg ferromagnet with planar anisotropy.⁵ CC2 can be described as a linear chain Ising ferromagnet. This was elegantly demonstrated by Torrance and Tinkham² who performed infrared transmission measurements at liquid-helium temperatures as a function of magnetic field in the easy direction of magnetization. Their experiments showed the existence of bound multimagnon states which are unique to this model and which correspond to a strikingly simple physical picture, namely, the flipping of clusters of adjacent spins along the Ising chain. Such excitations only break the bonds at the end of the cluster and should therefore have the same energy as the single spin flip in zero field. In a finite field the excitation energies should increase linearly with the field and with the size of the clusters. These features are seen quite clearly by Torrance and Tinkham.² A subsequent experiment by Nicoli and Tinkham⁶ employing laser

techniques has shown the existence of clusters with as many as 14 adjacent spins.

CC2 orders magnetically at 17.2 K. The spontaneous order is ferromagnetic within the chains and antiferromagnetic between chains. The spins align in the b^* direction.⁷ The coupling between the chains is weak, and moderate longitudinal external fields can modify the magnetic order. At $H_{c1} = 31$ kG the structure becomes ferrimagnetic with the spins in two out of three chains parallel to the field direction; at $H_{c2} = 45$ kG (at 4.2 K) all spins align, i. e., the system becomes ferromagnetic.^{1,2,7}

Multimagnons are observed in all three phases and the same conceptually simple picture can be applied. There are slight complications for the antiferromagnetic and antiferrimagnetic states due to the presence of additional ground-state modes with different Zeeman energies and due to the molecular fields created by the neighboring chains. However, this can easily be incorporated in the model, and Fig. 1, which is reproduced from the work of Torrance and Tinkham,² illustrates how closely the essentially one-dimensional Ising-model predictions correspond to the observed excitation spectrum. The details of the observations cannot be explained on basis of the Ising picture alone, especially since the multimagnon states are observable only because of additional terms in the Hamiltonian. Taking into account both the Heisenberg nature of the exchange and its transverse anisotropy, Torrance and Tinkham² obtained an excellent agreement between their optical data and a model Hamiltonian with a number of phenomenological parameters. The aim of the present work is to establish the dispersion of the magnetic excitation spectrum throughout the Brillouin zone by the use of inelastic neutron scattering. This will test the general validity of the Ising picture as well as the relevance of the phenomenological exchange parameters.

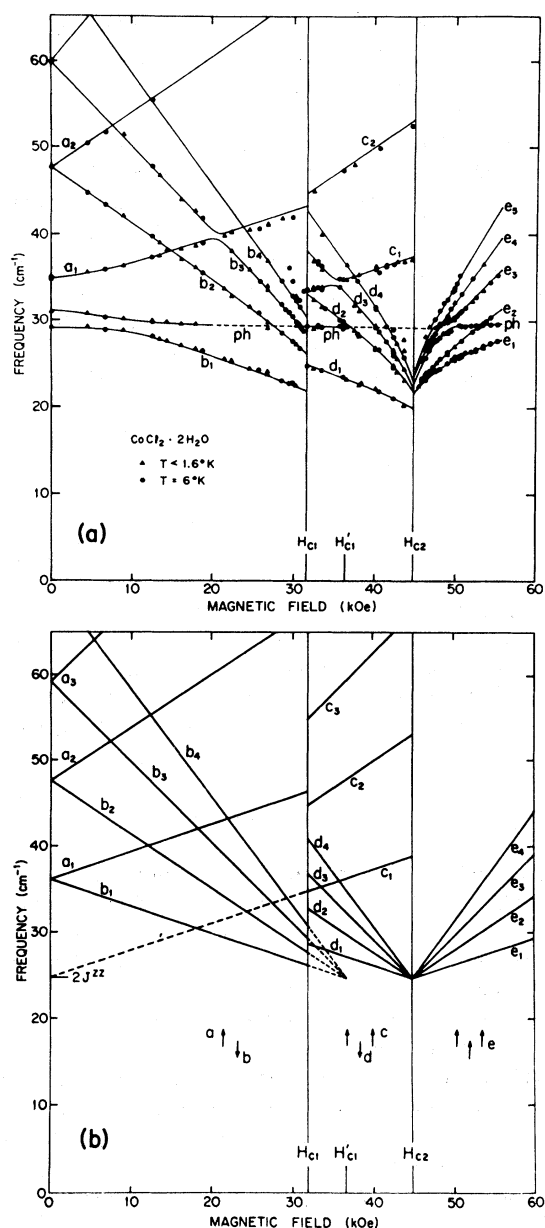


FIG. 1. Reproduction of the results by Torrance and Tinkham (Ref. 2) for $\text{CoCl}_2 \cdot 2\text{H}_2\text{O}$. (a) The observed resonance frequencies are plotted against the magnetic field H_0 which is applied along the b axis. The lines are the results of detailed theoretical calculations. (b) The simple Ising-model excitation spectra for spin clusters in the chains of $\text{CoCl}_2 \cdot 2\text{H}_2\text{O}$. The branch labels a , b , c , d , and e refer to excitations pertaining to the different sublattices in the three phases. Subscripts refer to cluster sizes. An optical phonon which hybridizes with the magnetic excitations is labeled ph .

II. EXPERIMENTAL DETAILS

$\text{CoCl}_2 \cdot 2\text{D}_2\text{O}$ ($\text{CoCl}_2 \cdot 2\text{H}_2\text{O}$) crystallizes in a monoclinic structure $C_{2/m}$ (No. 12 in the International Tables of Crystallography) with cell dimen-

sions⁸ $a = 7.306 \text{ \AA}$, $b = 8.498 \text{ \AA}$, $c = 3.564 \text{ \AA}$, and $\beta = 97.60$ at 5 K. This cell contains two formula units, whereas the primitive cell only contains one. The atomic positions are shown schematically in Fig. 2. The Néel temperature is 17.2 K, and the spontaneous antiferromagnetic structure is also illustrated in Fig. 2.

Single crystals are grown from solution by slow evaporation; the samples for the present experiments were provided by D. F. Nicoli. The crystals grow in rodlike shapes in which the c axis coincides with the rod axis. The faces of the rods are (110) and $(\bar{1}\bar{1}0)$, and only crystals with visible imperfections were found to exhibit twinning. Typical sample dimensions were $40 \times 4 \times 4 \text{ mm}^3$. The major part of the measurements were performed on a composite sample consisting of three such crystals whose crystallographic axes were aligned to within 1.5° . The composite sample was oriented so that $[010]$ and $[001]$ were in the scattering plane. Measurements on a single rod were made with $[100]$ and $[010]$ in the scattering plane.

The neutron scattering properties of CC2 are not ideal. The incoherent cross section per primitive cell is 20 b even for the fully deuterated sample, and the absorption length at a neutron energy of 15 meV is 7.4 mm corresponding to 130 b/(primitive cell), whereas the transverse

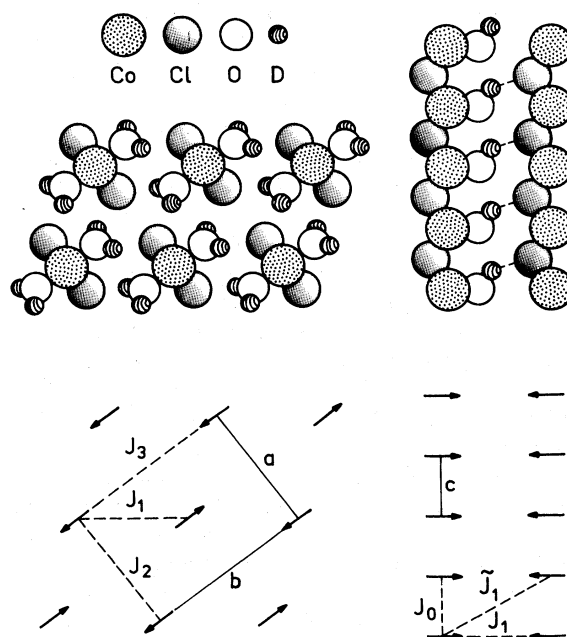


FIG. 2. Illustrations of the crystal structure and the simple antiferromagnetic structure of $\text{CoCl}_2 \cdot 2\text{D}_2\text{O}$. The left-hand sides correspond to projections on a $(00l)$ plane; and the right-hand sides correspond to projections on a (hko) plane. In the lower part, the lattice parameters and the exchange-model parameters are indicated.

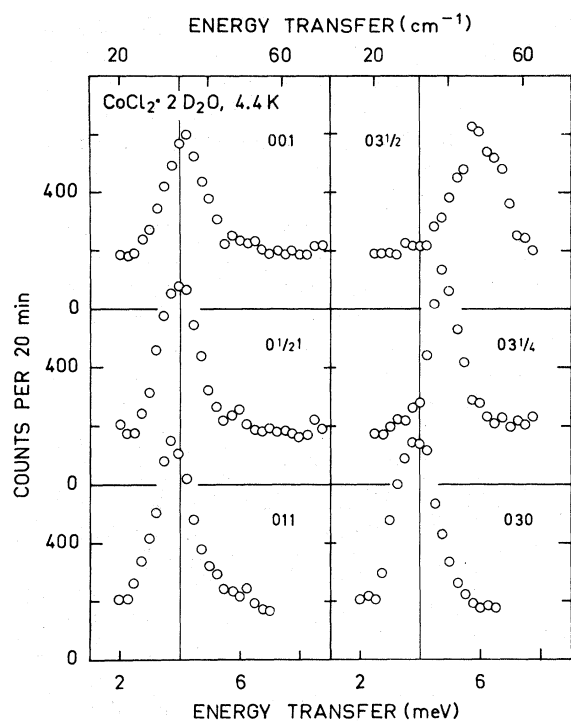


FIG. 3. Examples of the inelastic neutron-scattering scans along the b^* axis (left-hand side) and along the c^* axis (right-hand side).

magnetic cross section corresponds to only 4.2 b. The absorption causes the scattered intensity to vary with both sample geometry and scattering angle; this effect is especially large for the shape and orientation of the composite sample. This means that the intensity information can be used only after considerable and somewhat uncertain corrections. The relatively small magnetic cross section is more or less inherent to the class of systems consisting of chains of magnetic ions isolated by nonmagnetic ions and molecules; this dilution limits the amount of information that can be obtained from a neutron scattering experiment. Hence with respect to intensity and resolution the present study of CC2 is inferior compared to the optical studies. The lack of energy resolution in a neutron scattering experiment is often compensated by the presence of structure factors which weight the excitation spectrum differently depending on which zone in reciprocal space is used for the measurements.⁹ In an antiferromagnet such as CC2 this may be used to separate the so-called optic and acoustic spin-wave modes, even if their energies are close lying compared to the energy resolution.

The measurements to be presented were performed on a triple-axis spectrometer at the Risø DR-3 reactor. The spectrometer worked in the constant Q mode, scanning the incident neutron

energy. The outgoing energy was fixed at 14.6 meV ($k_f = 2.657 \text{ \AA}^{-1}$), and higher-order contaminations were removed from the beam by means of a 5-cm-long pyrolytic graphite filter. The collimation throughout the spectrometer was about 1° . The (002) reflections from pyrolytic graphite single crystals, vertically focusing and planar, were used to monochromatize the incident and scattered beams, respectively. This spectrometer configuration gives an energy resolution of 1.4 meV (11 cm^{-1}), full width at half-maximum (FWHM), at an energy transfer of 4 meV (32 cm^{-1}). The samples were mounted in a Cryogenic Associates CT-14 variable-flow cryostat and the measurements were performed in the temperature range 4.2–130 K with a typical stability of ± 0.5 K.

III. EXPERIMENTAL RESULTS

The present experiments were performed without an external magnetic field and were concentrated in the ordered antiferromagnetic phase. T_N was coarsely determined by monitoring the Bragg intensity of a magnetic superlattice reflection, all samples were found to order at 17 ± 0.5 K, in agreement with the values of T_N quoted in the literature.^{1,2,7} The antiferromagnetic structure⁷ at 4.2 K (shown in Fig. 2) was confirmed by elastic diffraction measurements in the ab plane of the single-rod specimen.

Examples of the inelastic scans on the composite sample at 4.4 K is shown in Fig. 3. These scans are dominated by the one-magnon resonance. Within the sensitivity limit determined by the large incoherent background we cannot identify any scattering from bound-state magnons. The energy widths (FWHM) of the one-magnon peaks correspond roughly to the instrumental resolution, which was calibrated at the incoherent elastic peak as well as against a vanadium sample. The peak positions were determined from least-squares fits of Gaussian curves to the data points of each scan at a fixed wave vector. The results of these fits are shown in Fig. 4. One notices that the dispersion along c^* is quite pronounced and that the splitting of the two magnon branches (a and b modes in the notation of Ref. 2) vanishes with increasing wave vector in this direction. We can resolve these branches only because they are seen with different intensity in different zones, as we shall discuss in Sec. IV.

The peak positions derived from the fits of a single Gaussian curve to the zone-center ($q=0$) scans are $\hbar\omega_a = 3.82 \pm 0.1$ meV ($30.8 \pm 1 \text{ cm}^{-1}$) at magnetic superlattice points and $\hbar\omega_b = 4.15 \pm 0.1$ meV ($33.5 \pm 1 \text{ cm}^{-1}$) at the nuclear reciprocal-lattice points. The corresponding frequencies derived from optical experiments² are 3.61 ± 0.01 meV ($29.15 \pm 0.1 \text{ cm}^{-1}$) and 4.32 ± 0.01 meV

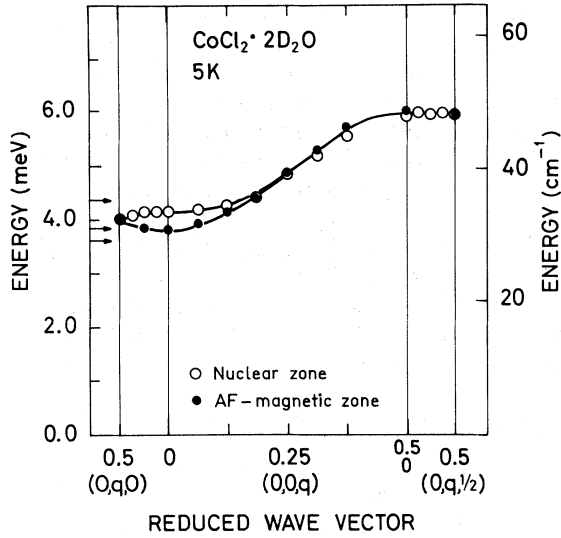


FIG. 4. Observed one-magnon excitation energies along three directions in reciprocal space. The energies have been determined from least-squares Gaussian fits to the inelastic scans. The solid lines are guides to the eye. The arrows indicate the observed peak positions from Ref. 2.

($34.9 \pm 0.1 \text{ cm}^{-1}$), which have a larger separation than the frequencies determined from the neutron scans. However, our scans may be fitted equally well by two Gaussian curves centered at the optic frequencies, using the relative weight of these curves as a fitting parameter. The result is a relative weight of 3:1 in fits where the known resolution width is used for the Gaussians. Hence the discrepancy between the optic results and the neutron data can be resolved by assuming that the two magnon branches are observed simultaneously but with different intensities in the neutron experiment. This is consistent with the description to be presented in Sec. IV.

The optical data (Fig. 1) show that the one-magnon states hybridize with an optical phonon whose zone-center frequency is about 3.7 meV (30 cm^{-1}), quite close to the b_1 magnon. There is no sign of this mode in the neutron data partly because of the poorer energy resolution and partly because the measurements were performed at relatively small scattering vectors where the pure phonon cross section is small (it scales with the square of the momentum transfer).

Some of the scans were repeated at increasing temperature and the results for the superlattice point 030 are shown in Fig. 5. There is a rapid shift and broadening in energy as T_N is approached, but a well-defined resonance persists above T_N where the broadening increases only slowly with temperature. We could not identify any quasielas-

tic magnetic scattering on top of the large incoherent elastic background scattering.

IV. SPIN-WAVE THEORY

The Torrance-Tinkham Hamiltonian² for CC2 has the form

$$H = - \sum_{i,\delta} [J_{\delta}^z S_i^z S_{i+\delta}^z + \frac{1}{2} J_{\delta}^{\pm} (S_i^+ S_{i+\delta}^- + S_{i+\delta}^+ S_i^-)] + \sum_i g_2 \mu_B H_z S_i^z, \quad (1)$$

with

$$J_{\delta}^{\pm} = \frac{1}{2} (J_{\delta}^x + J_{\delta}^y) \quad \text{and} \quad J_{\delta}^a = \frac{1}{2} (J_{\delta}^x - J_{\delta}^y),$$

where i numerates the Co^{+2} sites and δ specifies the relevant neighbors. The longitudinal anisotropy makes the first term, the Ising term, the dominating one. The exchange couplings that were used in Ref. 2 to calculate the exciton spectrum shown as the full curves in Fig. 1(a) are indicated in Fig. 2, and the parameter values are listed in Table I. The calculation by Torrance and Tinkham was based on up to forty eigenfunctions of the Ising Hamiltonian admixed by the transverse anisotropy. Fogedby¹⁰ has shown that the eigenvalue problem has exact analytic solutions when all orders of the multimagnons are included. In the present case of antiferromagnetic phase without external fields, it turns out that the multimagnons play a minor role and that the problem can be simplified considerably by reasonable approximations. A general, bilinear exchange Hamilton like Eq. (1) can be diagonalized straightforwardly in the random-

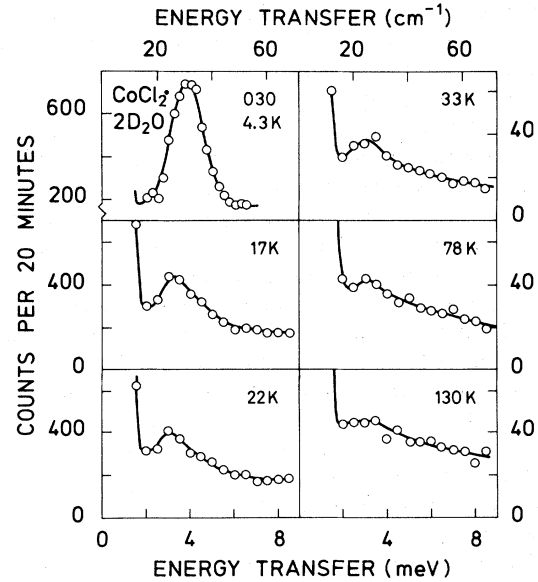


FIG. 5. Observed temperature dependence of the one-magnon peak at 030. The solid lines are merely guides to the eye.

TABLE I. Values for exchange parameters used by Torrance and Tinkham² to calculate theoretical excitation spectrum shown in Fig. 1 (a) for $\text{CoCl}_2 \cdot 2\text{H}_2\text{O}$. E_{ph} refers to the unperturbed optic phonon and $j_i^\alpha = J_i^\alpha / J_i^z$.

Parameter	Value
g_z	6.81 ± 0.10
H_{c1}	31.0 ± 0.3 kOe
H_{c2}	44.9 ± 0.3 kOe
H_3	0.3 ± 0.1 kOe
J_0^{zz}	12.66 ± 0.1 cm^{-1}
J_1^{zz}	-3.25 ± 0.1 cm^{-1}
J_2^{zz}	-0.7 ± 0.1 cm^{-1}
J_3^{zz}	0.09 ± 0.04 cm^{-1}
j_0^z	0.155 ± 0.01
$j_1^z = j_2^z$	0.280 ± 0.01
j_0^y	0.10 ± 0.01
$j_1^y = j_2^y$	0.16 ± 0.02
E_{ph}	29.3 ± 0.2 cm^{-1}
A_{AF}	0.55 ± 0.05 cm^{-1}

phase approximation, a procedure for deriving the neutron scattering cross sections has been given by Lindgård *et al.*¹¹ However, the general treatment sometimes obscures the physical arguments; in the following we shall present a simple Green's-function solution of the same problem, especially adapted to CC2 (for details see the Appendix).

In the antiferromagnetic (AF) phase CC2 exhibits two spin waves pertaining to each sublattice. The two AF modes, a and b , have Zeeman energies $\pm g_z \mu_B H_0$, respectively. In the absence of transverse anisotropy (J^a) and transverse mean exchange (J^\perp), the modes are undispersed and degenerate at vanishing field. They are separated from the ground-state energy by an amount $2J^z = 2 \sum_{\delta} J_{\delta}^z$ (of order 40 cm^{-1}). The transverse mean exchange (the Heisenberg exchange) along the chain gives rise to the usual spin-wave dispersion $-J_0^z \cos(\vec{k} \cdot \vec{c})$ common to both AF modes. The Heisenberg exchange between neighboring chains, however, can take place only if a pair of spin deviations is already virtually excited in the AF ground state. This contribution is therefore suppressed by a factor J^a/J^z of order $\frac{1}{10}$ and we shall neglect it. Similar considerations apply to the transverse anisotropy along the chains. In the AF phase the ground state and the higher multimagnon bound states are separated from the AF modes (at least at low field) by amounts of order 20 – 30 cm^{-1} ; the admixture effects due to J^a (of order a few cm^{-1}) are therefore negligible. The transverse anisotropy

between chains, however, lifts the zero-field degeneracy of the AF modes to linear order in J^a (at zero wavenumber ~ 5 cm^{-1}).

The antiferromagnetic magnons are directly observable by means of inelastic neutron scattering (selection rule $\Delta m = 1$). The neutrons measure the spin correlation function in the combination

$$S(\vec{k}, \omega) = \sum_{\alpha, \beta} \left(\delta_{\alpha\beta} - \frac{\kappa_{\alpha}\kappa_{\beta}}{\kappa^2} \right) g_{\alpha} g_{\beta} S^{\alpha\beta}(\vec{k}, \omega), \quad (2)$$

where ω and \vec{k} are the energy and momentum transfers, respectively. The spin correlation function is defined as follows:

$$S^{\alpha\beta}(\vec{k}, \omega) = \sum_{ij} \int dt e^{i\omega(t-t')} \times e^{-i\vec{k} \cdot (\vec{x}_i - \vec{x}_j)} \psi_0^* S_i^{\alpha}(t) S_j^{\beta}(t') \psi_0. \quad (3)$$

α and β are the Cartesian components x , y , and z . The site indices i and j run over the whole lattice (both sublattices). ψ_0 is an appropriately chosen ground state. Note that in the presence of an energy gap of order 30 cm^{-1} , temperature effects are exponentially small. Referring to the discussion above we choose as ground state the Ising AF state. Denoting the two sublattices by A and B , i. e.,

$$S_A^b \psi_0 = -S_B^b \psi_0 = \frac{1}{2} \psi_0 \quad \text{and} \quad S_A^+ \psi_0 = S_B^- \psi_0 = 0,$$

we easily see that the only nonvanishing components of the spin correlation function are S_{AA}^{++} , S_{AB}^{++} , S_{BA}^{--} , and S_{BB}^{--} . We have as usual introduced the lowering and raising operators $S^{\pm} = S^x \pm iS^y$. In the appendix we evaluate the spin correlation function (3) within the framework of the approximations discussed above.

The spin-wave energies $\tilde{\omega}_a(\vec{k})$ and $\tilde{\omega}_b(\vec{k})$ are given by

$$\hbar \tilde{\omega}_{a,b}(\vec{k}) = J^z - J^{\perp}(\vec{k}) \pm J^a(\vec{k}), \quad (4)$$

where we have introduced the exchange energies

$$J^z = \sum_{\delta, \delta'} J_{\delta}^z, \quad J^{\perp} = \sum_{\delta} J_{\delta}^{\perp} e^{i\vec{k} \cdot \vec{x}_{\delta}}$$

and

$$J^a(\vec{k}) = \sum_{\delta'} J_{\delta'}^a e^{i\vec{k} \cdot \vec{x}_{\delta'}}. \quad (5)$$

δ and δ' denote summation over the two sublattices, respectively. For the full spin correlation function $S = S_{AA} + S_{AB} + S_{BA} + S_{BB}$ we obtain finally

$$S(\vec{k}, \omega) = (1 - \kappa_x^2/\kappa^2) g_x^2 \pi \delta(\omega - \tilde{\omega}_a(\vec{k})) + (1 - \kappa_y^2/\kappa^2) g_y^2 \pi \delta(\omega - \tilde{\omega}_b(\vec{k})). \quad (6)$$

V. DISCUSSION

The orientation of the g tensor in CC2 is not entirely fixed by symmetry. It has been determined by Narath¹ from nuclear magnetic resonance and

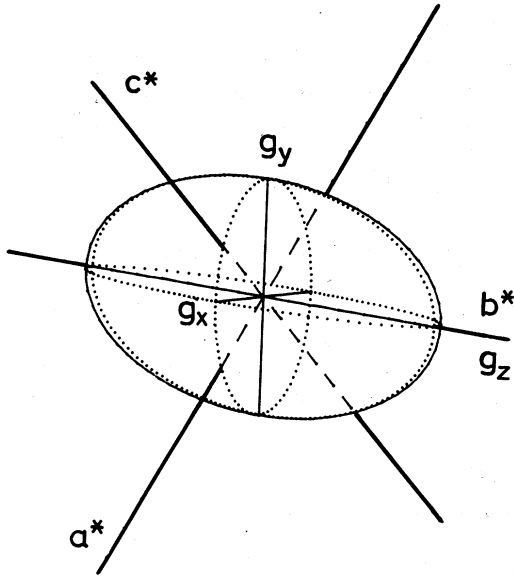


FIG. 6. Illustration of the anisotropy and the orientation of the g tensor relative to the crystal coordinates based on the parameter values derived by Narath (Ref. 1).

susceptibility measurements paired with crystal-field calculations. The relative positions of the crystal axes and the principal axes of the g tensor is shown in Fig. 6. The z axis coincides with b^* and the x and y axes coincide approximately with the $\text{Co}^{+2}-\text{Cl}^-$ bonds. The angle between y and c^* is 55° . The sizes of the major axes in the ground state are $g_x = 1.87$, $g_y = 3.32$, and $g_z = 6.77$. This means that the two terms in Eq. (6) have significantly different weights besides the polarization factor. In a measurement with $\vec{\kappa}$ along $[0k0]$, i. e., $\kappa_x = \kappa_y = 0$, one should observe the resonance with the intensity ratio 1:3. A measurement along $[00l]$ gives $\kappa_x/\kappa = \cos(35)$ and $\kappa_y/\kappa = \sin(35)$, and hence an expected intensity ratio of 1:6.

The exchange-constant model (Table I and Fig. 2) which was used by Torrance and Tinkham² to fit their data (Fig. 1), does not give an adequate description of the observed dispersion. The predicted over-all dispersion is too small and the splitting of the a and b spin waves along c^* is predicted to be constant. We can remedy this in the model somewhat by changes in the parameter values and by postulating an additional coupling between the chains, \vec{J}_1 , as illustrated in Fig. 2. A physical argument for this coupling can be produced by consideration of the superexchange path between the chains (see Fig. 2). It involves a water molecule and a Cl^- ion which is equally close to the two Co^{+2} ions that are connected by \vec{J}_1 and \vec{J}_1 . Consequently, there is an equal number of links of the two types and one would estimate their effects to be equal. Thus

TABLE II. Exchange energies and parameter values determined from model fits to the observed dispersion curves.

[meV (cm^{-1})]	[meV (cm^{-1})]
$J^a = 5.05 \pm 0.05$ (40.8 \pm 0.4)	$J_0^{aa} = 1.6$ (12.9) ^a
$J^\perp(0) = 0.95 \pm 0.05$ (7.7 \pm 0.4)	$J_0^\perp = 0.48 \pm 0.03$ (3.8 \pm 0.2)
$J^a(0) = 0.15 \pm 0.05$ (1.2 \pm 0.4)	$J_1^a = J_1^\perp = 0.02 \pm 0.01$ (0.2 \pm 0.1)

^aAssumes $J_1^a/J_1^\perp = 0.16$, Ref. 2.

$$J^a(\vec{\kappa}) = 4 \cos(\frac{1}{2}\vec{\kappa} \cdot \vec{a}) \cos(\frac{1}{2}\vec{\kappa} \cdot \vec{b}) \times [J_1^a + \vec{J}_1^a \cos(\kappa \cdot \vec{c})], \quad (7)$$

$$J^z = 2J_0^z - 4J_1^z - 4\vec{J}_1^z,$$

and

$$J^\perp(\vec{\kappa}) = 2J_0^\perp \cos(\vec{\kappa} \cdot \vec{c}),$$

where we have neglected J_2 and J_3 . The agreement one thus achieves with the observed exchange energies is illustrated in Fig. 7. The parameter values for the calculated lines are given in Table II. The over-all dispersion $J^\perp(\vec{\kappa})$ is well represented by the model cosine curve, whereas the anisotropic component $J^a(\vec{\kappa})$ is observed to fall off with increasing wave vector more rapidly than predicted by the two-parameter model. This suggests that the anisotropic transverse interaction between the chains might originate in mechanisms other than superexchange. The orbital moment of Co^{+2} is not quenched in CC2 and hence an obvious source of such interaction is the phonon induced quadru-

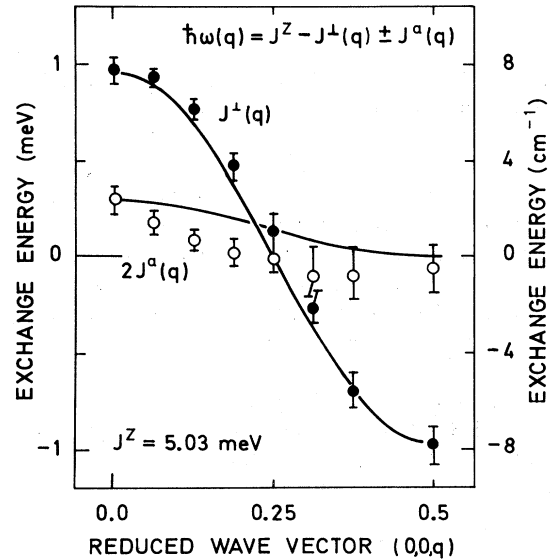


FIG. 7. Analysis of the observed dispersion according to the expression for the dispersion derived in the text, $\hbar\omega(q) = J^z - J^\perp(q) \pm J^a(q)$. The solid lines are model calculations based on the parameter values given in Table II.

pole coupling which is known from rare-earth insulators.¹² This interaction is strain mediated and hence it is more typical of longer range than superexchange. In reciprocal space it means that the effect is largest at small wave vectors. The optical work on CC2 has shown that there is a phonon-magnon coupling of magnitude similar to the observed splitting between the *a* and *b* one-magnon modes. Since the point symmetry is low, there are many optical phonons that in principle could contribute to such a coupling.

The present study of $\text{CoCl}_2 \cdot 2\text{D}_2\text{O}$ has corroborated the general physical picture which was derived from the optical experiments. The Heisenberg nature of the intrachain exchange interaction is found to be larger than previously assumed, but the Ising term remains the dominating one. The less-certain transverse anisotropy in the interaction between the chains is found to be of relatively long range.

The temperature dependence of the inelastic spectra (Fig. 5) shows that correlation along the Co^{+2} chains persists at temperatures which are high compared to T_N , where three-dimensional order sets in. This matches observations for other magnetic-chain compounds.^{3,5}

The bound magnon states were not observed. This is partly because of the lack of sensitivity in elastic neutron scattering experiments compared to the optical ones, and partly because the measurements were carried out at zero external field where the mixing and hence the cross section is small.

ACKNOWLEDGMENT

It is a pleasure to acknowledge P. -A. Lindgård for his contributions to spin-wave analysis.

APPENDIX

Here we evaluate the various nonvanishing components of the spin correlation function employing a Green's-function formalism. This will enable us to obtain the intensities of the observed lines and their positions directly, without necessitating the computation of wave functions as an intermediate step.

Let us denote the spin operators pertaining to the *A* and *B* sublattices by S_A and S_B , respectively. S_A and S_B commute, and each set satisfies the usual commutation relations

$$[S_i^+, S_j^+] = \mp \hbar S_i^+ \delta_{ij}, \quad (\text{A1})$$

$$[S_i^-, S_j^+] = -2\hbar S_i^z \delta_{ij}, \quad (\text{A2})$$

together with the length condition

$$S_i^+ S_i^- - S_i^z = \frac{1}{2} \quad (\text{A3})$$

and the minimum equations

$$S_i^+ S_i^+ = S_i^- S_i^- = 0, \quad S_i^z S_i^z = \frac{1}{4}. \quad (\text{A4})$$

The equation of motion for S_j^- is $i\hbar \dot{S}_j = [S_j, H]$, or written fully using the Hamiltonian (1) together with the commutation relations (A1) and (A2),

$$i \frac{d}{dt} S_j^- = - \sum_{\delta} (2J_{\delta}^z S_{j+\delta}^z - g_z \mu_B H_z) S_j^- + \sum_{\delta} (2J_{\delta}^+ S_j^z) S_{j+\delta} + \sum_{\delta} (2J_{\delta}^z S_{\delta}^z) S_{j+\delta}^+. \quad (\text{A5})$$

In order to provide an initial condition for the equations of motion for the spin correlation function, it is convenient to introduce the retarded spin correlation function (i.e., a retarded Green's function)

$$\tilde{S}(\vec{k}, t) = 2i S(\vec{k}, t) \eta(t), \quad (\text{A6})$$

where $\eta(t)$ is the step function

$$\eta(t) = \begin{cases} 0, & t < 0 \\ 1, & t > 0. \end{cases}$$

Keeping in mind that $d\eta(t)/dt = \delta(t)$, we obtain the following Fourier-transformed equations of motion for the nonvanishing components of the retarded spin correlation function:

$$\begin{aligned} (\omega_a(\vec{k}) - i \frac{d}{dt}) \tilde{S}_{AA}^{+-}(\vec{k}, t) &= 2\delta(t) + J^a(\vec{k}) \tilde{S}_{BA}^{--}(\vec{k}, t), \\ (\omega_a(\vec{k}) - i \frac{d}{dt}) \tilde{S}_{AB}^{++}(\vec{k}, t) &= J^a(\vec{k}) \tilde{S}_{BB}^{+-}(\vec{k}, t), \\ (\omega_b(\vec{k}) - i \frac{d}{dt}) \tilde{S}_{AA}^{--}(\vec{k}, t) &= J^a(\vec{k}) \tilde{S}_{AA}^{+-}(\vec{k}, t), \\ (\omega_b(\vec{k}) - i \frac{d}{dt}) \tilde{S}^{--}(\vec{k}, t) &= 2\delta(t) + J^a(\vec{k}) \tilde{S}_{AB}^{++}(\vec{k}, t). \end{aligned} \quad (\text{A7})$$

Here

$$\begin{aligned} \hbar \omega_{a,b}(\vec{k}) &= J^z - J^{\perp}(\vec{k}) \pm g_z \mu_B H_z, \\ J^z &= \sum_{\delta, \delta'} J_{\delta}^z, \quad J^{\perp}(\vec{k}) = \sum_{\delta} J_{\delta}^{\perp} e^{i\vec{k} \cdot \vec{x}_{\delta}}, \\ J^a(\vec{k}) &= \sum_{\delta'} J_{\delta}^a e^{i\vec{k} \cdot \vec{x}_{\delta'}}, \end{aligned} \quad (\text{A8})$$

where δ and δ' run over the two sublattices, respectively.

Finally a comment about the Fourier transforms $S_{AB}(\vec{k}, t)$, etc., are defined as follows:

$$S_{AB}^{\alpha\beta}(\vec{k}, t) = \sum_{\substack{i \in A \\ j \in B}} e^{-i\vec{k} \cdot (\vec{x}_i - \vec{x}_j)} \psi_0^{\alpha} S_{A,i}^{\alpha}(t) S_{B,j}^{\beta}(0) \psi_0. \quad (\text{A9})$$

The linear equations of motion (A7) are readily solved by a Laplace transformation. Noting that the Laplace transform of (A6) is

$$\tilde{S}(\vec{k}, z) = \int \frac{d\omega}{\pi} \frac{S(\vec{k}, \omega)}{\omega - z} \quad (\text{A10})$$

and that the physically observable (in neutron scattering) correlation function $S(\vec{k}, \omega)$ is obtainable as the limit

$$\lim_{z \rightarrow \omega + i\epsilon} \text{Im} \tilde{S}(\vec{k}, z) = S(\vec{k}, \omega), \quad (\text{A11})$$

we get in the absence of a magnetic field

$$\begin{aligned} \tilde{S}_{AA}^{+-} &= \tilde{S}_{BB}^{+-} = (\tilde{\omega}_a - z)^{-1} + (\tilde{\omega}_b - z)^{-1}, \\ \tilde{S}_{AB}^{++} &= \tilde{S}_{BA}^{--} = (\tilde{\omega}_a - z)^{-1} - (\tilde{\omega}_b - z)^{-1}, \end{aligned} \quad (\text{A12})$$

and consequently

$$\begin{aligned} S_{AA}^{+-}(\vec{k}, \omega) &= S_{BB}^{+-}(\vec{k}, \omega) \\ &= \pi[\delta(\omega - \tilde{\omega}_a(\vec{k})) + \delta(\omega - \tilde{\omega}_b(\vec{k}))], \\ S_{AB}^{++}(\vec{k}, \omega) &= S_{BA}^{--}(\vec{k}, \omega) \\ &= \pi[\delta(\omega - \tilde{\omega}_a(\vec{k})) - \delta(\omega - \tilde{\omega}_b(\vec{k}))], \end{aligned} \quad (\text{A13})$$

when the perturbed spin-wave energies $\tilde{\omega}_{a,b}$ are given by $[\omega_a(\vec{k}) = \omega_b(\vec{k}) = \omega(\vec{k})]$

$$\hbar \tilde{\omega}_{a,b}(\vec{k}) = \hbar \omega(\vec{k}) \pm J^a(\vec{k}). \quad (\text{A14})$$

*Visiting scientist at AEK Risø, Denmark.

¹A. Narath, Phys. Rev. **140**, A552 (1965).

²J. B. Torrance, Jr. and M. Tinkham, Phys. Rev. **187**, 587 (1969); **187**, 595 (1969).

³M. T. Hutchings, G. Shirane, R. J. Birgeneau, and S. L. Holt, Phys. Rev. B **5**, 1999 (1972).

⁴J. Skalyo, Jr., G. Shirane, S. A. Friedberg, and H. Kobayashi, Phys. Rev. B **2**, 4632 (1970).

⁵M. Steiner and B. Dorner, Solid State Commun. **12**, 537 (1973).

⁶D. F. Nicoli and M. Tinkham, Phys. Rev. B **9**, 3126 (1974).

⁷D. E. Cox, B. C. Frazer, and G. Shirane, Phys. Lett. **17**, 103 (1965); D. E. Cox, G. Shirane, and A. Narath, J. Appl. Phys. **37**, 1126 (1966).

⁸Bruno Morosin, J. Chem. Phys. **44**, 252 (1966).

⁹See, for example, W. Marshall and S. W. Lovesey, *Theory of Thermal Neutron Scattering* (Clarendon, Oxford, 1971).

¹⁰H. C. Fogedby, Phys. Rev. B **10**, 4000 (1974).

¹¹P.-A. Lindgård, A. Kowalska, and P. Laut, J. Phys. Chem. Solids **28**, 1357 (1967).

¹²G. A. Gehring and K. A. Gehring, Rep. Prog. Phys. **38**, 1 (1975).